A NUMERICAL STUDY OF DRAG AND HEAT TRANSFER TO BLUNT NOSE SHAPES IN RAREFIED HYPERSONIC FLOW

Wilson F. N. Santos
Combustion and Propulsion Laboratory
National Institute for Space Research
Cachoeira Paulista, SP 12630-000 Brazil

Keywords: *Hypersonic flow, Rarefied Flow, DSMC, Blunt leading edge, Aerodynamic heating*

Abstract

The steady-state aerodynamic characteristics of a new family of blunted leading edges immersed in high-speed rarefied air flow are examined by using a Direct Simulation Monte Carlo (DSMC) method. The work is motivated by interest in investigating the flowfield properties of these new blunt shapes as possible candidates for blunting geometries of hypersonic leading edges. Comparisons are made between these new blunt configurations and round shapes based on stagnation point heating and total drag. Some significant differences between these shapes is noted on the aerodynamic surface quantities. It was found that round leading edges provided smaller stagnation point heating than the new blunt leading edges. The analysis also shows that, despite the seeming advantages of the new blunt shapes, round shapes still provides smaller stagnation point heating, however large total drag under the range of conditions investigated.

1 Introduction

At hypersonic flight speeds, the vehicle leading edges must be blunt to some extent in order to reduce the heat transfer rate to acceptable levels and to allow for internal heat conduction. The use of blunt-nose shapes tends to alleviate the aerodynamic heating problem since the heat flux for blunt bodies is far lower than that for sharply pointed bodies. In addition, the reduction in heating rate for a blunt body is accompanied by an increase in heat capacity, due to the increased volume. Due mainly to manufacturing problems and the extremely high temperatures attained in hypersonic flight, hypersonic vehicles will have blunt nose, although probably slendering out at a short distance from the nose. Therefore, designing a hypersonic vehicle leading edge involves a tradeoff between making the leading edge sharp enough to obtain acceptable aerodynamic and propulsion efficiency and blunt enough to reduce the aerodynamic heating in the stagnation point.

A method of designing low heat transfer bodies is devised on the premise that the rate of heat transfer to the nose will be low if the local velocity is low, while the rate of heat transfer to the afterbody will be low if the local density is low (Reller [1]). A typical body that results from this design method consists of a flat nose followed by a highly curved, but for the most part slightly inclined, afterbody surface.

The emphasis of this work is to compare these new contours (flat-nose leading edge) with round leading edges in order to determine which geometry is better suited as a blunting profile in terms of stagnation point heating and total drag coefficient. Two method of comparing these shapes to round leading edges will be investigated:(1) flat-nose leading edges are compared to a corresponding round leading edge (circular cylinder), which generates the flat-nose shapes, and (2) flat-nose leading edges are compared to an equivalent round leading edge, which is generated from the computational results for the flat-nose shapes. The equivalent round leading edge will yield either the same stagnation point heating or the same drag coefficient as the computed solutions presented for flat-nose shapes. Thus, for the equivalent stagnation point heating, for instance, the total drag coefficient will be the basis of comparison between these leading edges, and they will determine which geometry performs better.

The focus of the present study is the low-density region in the upper atmosphere, where numerical gas-kinetic procedures are available to simulate hypersonic flows. High-speed flows under low-density conditions deviate from a perfect gas behavior because of the excitation of rotation, vibration and dissociation. At high altitudes, and therefore low density, the molecular collision rate is low and the energy exchange occurs under non-equilibrium conditions. In such a circumstance, the degree of molecular non-equilibrium is such that the Navier-Stokes equations are inappropriate. Alternatively, the Direct Simulation Monte Carlo method will be employed to calculate the rarefied hypersonic two-dimensional flow on the leading edge shapes.

2 Body Shape Definition

In dimensionless form, the contour that defines the shape of the afterbody surface is given by the following expression,

$$\bar{x} \;=\; \int_{1}^{\bar{y}_{max}} \sqrt{\bar{y}^{k}-1}\,d\bar{y} \qquad (1)$$

where $\bar{x} = x/y_{nose}$ and $\bar{y} = y/y_{nose}$.

The flat-nose leading edges are modeled by assuming a sharp leading edge of half angle θ with a circular cylinder of radius R inscribed tangent to this wedge. The flat-nose leading edges, inscribed between the wedge and the cylinder, are also tangent to them at the same common point where they have the same slope angle. It was assumed a leading edge half angle of 10 deg, a circular cylinder diameter of 10^{-2}m and flat-nose thicknesses t/λ_∞ of 0.01, 0.1 and 1, where $t = 2y_{nose}$ and λ_∞ is the molecular freestream mean free path. Figure 1 illustrates this construction for the set of shapes investigated. From geometric considerations, the exponent k in Eq.(1) is obtained by matching slope on the wedge, on the circular cylinder and on the body shapes at the tangency point. For dimensionless thicknesses of 0.01, 0.1 and 1, the exponent k corresponds to 0.501, 0.746 and 1.465, respectively. The common body height H and the body length L are obtained in a straightforward manner.

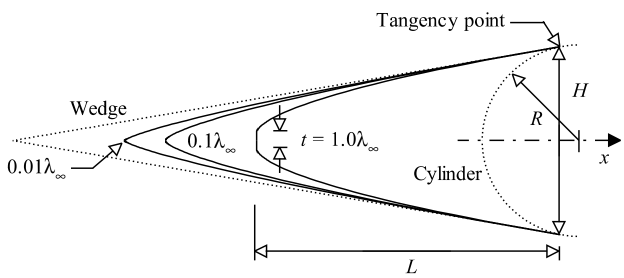

Fig. 1 Drawing illustrating the leading edge geometries.

3 Computational Method and Procedure

The degree of departure of a flow from the continuum is indicated by the flow Knudsen number, $Kn = \lambda/l$, where λ is the molecular mean free path and l is a characteristic length of the flow. Traditionally, flows are divided into four regimes (Schaff [2]): $Kn < 0.01$, continuum flow, $0.01 < Kn < 0.1$, slip flow, $0.1 < Kn < 10$, transitional flow, and $Kn > 10$, free molecular flow. It is well know that neither the continuum flow equations nor the collisionless flow equations are valid to predict leading edge aerothermodynamic characteristics throughout the transitional flow regime. At this time it appears that the Direct Simulation Monte Carlo (DSMC) method [3] is the most accurate and credible procedure for computing leading edge flowfield and surface effects in the transitional flow regime.

The DSMC method simulates real gas flows with various physical processes by means of a huge number of modeling particles, each of which is a typical representative of great number of real gas molecules. In the DSMC method, the state of the particles is stored and modified with time as the particles move, collide, and undergo boundary interactions in simulated physical space.

The molecular collisions are modeled using the variable hard sphere(VHS) molecular model [4]. The energy exchange between kinetic and internal modes is controlled by the Borgnakke-Larsen statistical model [5]. Simulations are performed using a non-reacting gas model consisting of two chemical species, N_2 and O_2. Energy exchanges between the translational and internal modes are considered. For this study, the relaxation numbers of 5 and 50 were used for the rotation and vibration, respectively.

The flowfield is divided into a number of regions, which are subdivided into computational cells. The cells are further subdivided into four subcells, two subcells/cell in each coordinate direction. The cell provides a convenient reference for the sampling of the macroscopic gas properties, while the collision partners are selected from the same subcell for the establishment of the collision rate. The linear dimensions of the cells should be small in comparison with the scale length of the macroscopic flow gradients normal to the streamwise directions, which means that the cell dimensions should be of the order of the local mean free path or even smaller [3]. Time is advanced in discrete steps such that each step is small in comparison with the mean collision time [3]. The simulation is always calculated as unsteady flow. However, a steady flow solution is obtained as the large time state of the simulation.

The computational domain used for the calculation is made large enough so that body disturbances do not reach the upstream and side boundaries, where freestream conditions are specified. A schematic view of the computational domain is depicted in Fig. 2. Side I is defined by the body surface. Diffuse reflection with complete thermal accommodation is the condition applied to this side. Advantage of the flow symmetry is taken into account, and molecular simulation is applied to one-half of a full configuration. Thus, side II is a plane of symmetry, where all flow gradients normal to the plane are zero. At the molecular level, this plane is equivalent to a specular reflecting boundary. Side III is the freestream side through which simulated molecules enter and exit. Finally, the flow at the downstream outflow boundary, side IV, is predominantly supersonic and vacuum condition is specified [3]. At this boundary, simulated molecules can only exit.

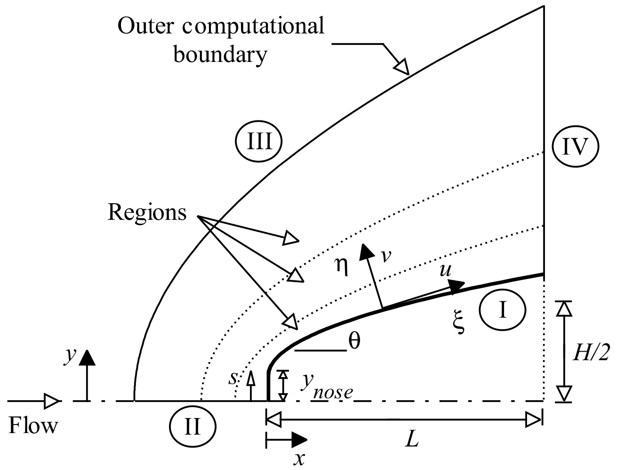

Fig. 2 Schematic view of the computational domain.

Numerical accuracy in DSMC method depends on the grid resolution chosen as well as the number of particles per computational cell. Both effects were investigated to determine the number of cells and the number of particles required to achieve grid independence solutions. Grid independence was tested by running the calculations with half and double the number of cells in ξ and η directions (see Fig. 2) compared to a standard grid. Solutions (not shown) were near identical for all grids used and were considered fully grid independent.

The freestream conditions and the gas properties used in the present simulation are those given by Santos [6] and summarized in Table 1.

The freestream velocity V_∞ is assumed to be constant at 3.56 km/s, which corresponds to freestream Mach number M_∞ of 12. The wall temperature T_w is assumed constant at 880 K. The

Table 1 Freestream and flow conditions

Parameter	Value	Unit
Temperature (T_∞)	220.0	K
Pressure (p_∞)	5.582	N/m^2
Density (ρ_∞)	8.753×10^{-5}	kg/m^3
Viscosity (μ_∞)	1.455×10^{-5}	Ns/m^2
Number density (n_∞)	1.8209×10^{21}	m^{-3}
Mean free path (λ_∞)	9.03×10^{-4}	m
Molecular mass O_2	5.312×10^{-26}	kg
Molecular mass N_2	4.650×10^{-26}	kg
Molecular diameter O_2	4.01×10^{-10}	m
Molecular diameter N_2	4.11×10^{-10}	m
Mole fraction O_2	0.237	
Mole fraction N_2	0.763	
Viscosity index O_2	0.77	
Viscosity index N_2	0.74	

overall Knudsen number Kn_t, defined as the ratio of the freestream mean free path λ_∞ to the leading edge thickness t, corresponds to 100, 10 and 1 for flat-nose thicknesses t/λ_∞ of 0.01, 0.1 and 1, respectively. The Reynolds number Re_t covers the range from 0.193 to 19.3, based on conditions in the undisturbed stream with leading edge thickness t as the characteristic length.

4 Computational Results and Discussion

The purpose of this section is to discuss differences in the heat transfer and total drag due to variations in the leading edge thickness and to compare them to round shapes. Comparisons based on geometry are made to examine the benefits and disadvantages of using these blunt geometries over round shapes.

4.1 Flat-Nose Shape

The heat flux q_w to the body surface is calculated by the net energy flux of the molecules impinging on the surface. The net heat flux is related to the sum of the translational, rotational and vibrational energies of both incident and reflected molecules. A flux is regarded as positive if it is directed toward the surface. The heat flux is normalized by the freestream kinetic energy flux $\rho_\infty V_\infty^3/2$ and presented in terms of heat transfer coefficient C_h.

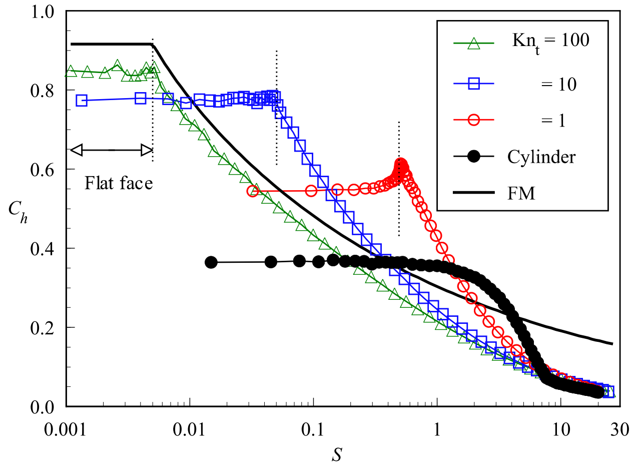

Fig. 3 Heat transfer coefficient along the body surface for blunt bodies.

The heat transfer coefficient C_h is illustrated in Fig. 3 as a function of the dimensionless arc length S ($\equiv s/\lambda_\infty$) along the surface measured from the stagnation point. For comparison purpose, Fig. 3 also illustrates the heat transfer coefficient for the reference round leading edge (circular cylinder) and the heat transfer coefficient by assuming free molecular flow. It is seen from this figure that the heat transfer coefficient is sensitive to the leading edge thickness. As would be expected, the blunter the leading edge the lower the heat transfer coefficient at the stagnation point. Also, the heat transfer coefficient remains essentially constant over the first half of the front surface, but then increases in the vicinity of the flat nose/afterbody junction for the bluntest case investigated, $Kn_t = 1$ ($t/\lambda_\infty = 1$). Subsequently, the heat transfer coefficient decreases sharply and continues to decline along the body surface. In contrast, for the circular cylinder, the heat transfer coefficient remains essentially constant over the first half of the cylindrically portion of the leading edge, but then decreases sharply up to the cylinder/wedge junction. Referring to Fig. 3, it is also observe that the heat transfer coefficient approaches the free molecular limit as the leading edge thickness decreases, i.e., as the Knudsen number Kn_t increases.

The heat transfer coefficient at the stagnation point C_{ho} was estimated as being 0.605, 0.730, and 0.785 for cases Kn_t of 100, 10 and 1, which correspond to the thickness t/λ_∞ of 0.01, 0.1 and 1, respectively. Furthermore, the heat transfer coefficient at the stagnation point for the reference round leading edge is C_{ho} = 0.366. Therefore, C_{ho} for the cases Kn_t of 100, 10 and 1 are 2.4, 2.2 and 1.5 times, respectively, larger than that for the reference round leading edge case.

The drag on a surface in a gas flow results from the interchange of momentum between the surface and the molecules colliding with the surface. The total drag is obtained by the integration of the pressure p_w and shear stress τ_w distributions along the body surface. In an effort to understand the effects of the pressure and the shear stress acting on the surface of the flat-nose leading edges, both forces will be presented in this section.

The pressure p_w on the body surface is calculated by the sum of the normal momentum fluxes of both incident and reflected molecules at each time step. Results are normalized by the freestream dynamic pressure $\rho_\infty V_\infty^2/2$ and presented in terms of pressure coefficient C_p.

The effects of the leading edge thickness on the pressure coefficient are demonstrated in Fig. 4. Plotted along with the computational solution for pressure coefficient is the pressure coefficient predicted by the free molecular flow equations and that for the circular cylinder used as a reference. Referring to Fig. 4, it can be seen that the pressure coefficient is basically constant along the front surface, and this constant value increases with increasing Knudsen number Kn_t. The pressure coefficient predicted by the free molecular flow equations on the front surface is 2.35. Therefore, for the thinnest blunt leading edge investigated, Kn_t of 100 (t/λ_∞ = 0.01), the flow seems to approach the free collision flow in the vicinity of the stagnation point. For the circular cylinder case, the pressure coefficient follows the same trend presented by the heat transfer coefficient in that it remains constant over the first half of the cylindrically portion of the leading edge, but then decreases sharply up to the cylinder/wedge junction.

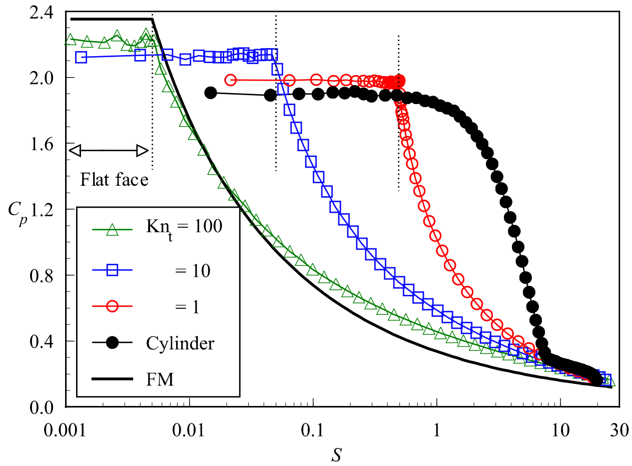

Fig. 4 Pressure coefficient along the body surface for blunt bodies.

The shear stress τ_w on the body surface is calculated by averaging the tangential momentum transfer of the molecules impinging on the surface. For the diffuse reflection model imposed for the gas-surface interaction, reflected molecules have a tangential moment equal to zero, since the molecules essentially lose, on average, their tangential velocity component. The shear stress τ_w is normalized by the freestream dynamic pressure $\rho_\infty V_\infty^2/2$ and presented in terms of the skin-friction coefficient C_f.

The influence of the leading edge thickness on the skin friction coefficient C_f is displayed in Fig. 5, parameterized by the thickness Knudsen number Kn_t. It is observed that the skin friction coefficient is zero at the stagnation point and slightly increases along the front surface up to the flat-nose/afterbody junction of the leading edge. After that, it increases dramatically to a maximum value that depends on the leading edge thickness, and decreases downstream along the body surface. Smaller thickness t (larger Kn_t) leads to higher peak value for the skin friction coefficient. Also, smaller thickness t displaces the peak value to near the front surface/afterbody junction.

Referring to Fig. 5, the skin friction coefficient predicted by the free molecular flow ex-

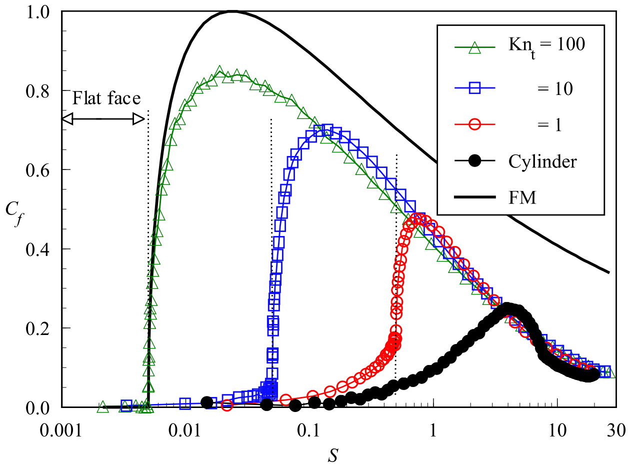

Fig. 5 Skin friction coefficient along the body surface for blunt bodies.

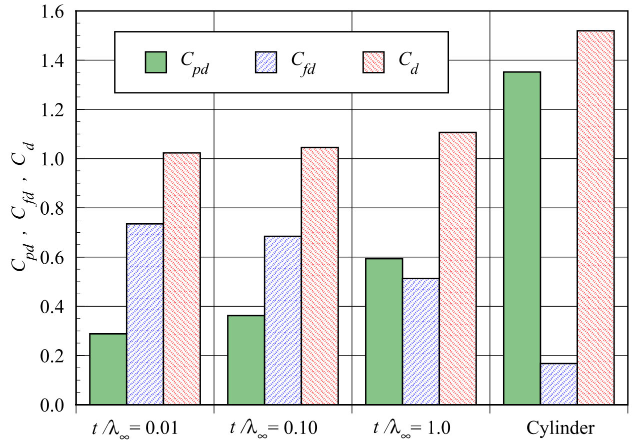

Fig. 6 Pressure drag, skin friction drag and total drag for flat-nose shapes and circular cylinder.

hibits its maximum value at a station that corresponds to a body slope of 45 degree. Similarly, the maximum values for the leading edge thicknesses investigated occur very close to the same station. Nevertheless, attention should be paid to the fact that the 45-degree station corresponds to different dimensionless arc length S for the leading edge thicknesses investigated, since the exponent k, that appears in Eq.(1), is different for each case.

The total drag is obtained by the integration of the pressure p_w and shear stress τ_w distributions from the nose of the leading edge to the station L (see Fig. 1), which corresponds to the tangent point common to all of the body shapes. It is important to mention that the values for the total drag presented in this section were obtained by assuming the shapes acting as leading edges. Consequently, no base pressure effects were taken into account on the calculations. The DSMC results for total drag are normalized by $\rho_\infty V_\infty^2 H/2$ and presented as total drag coefficient C_d and its components of pressure drag C_{pd} and skin friction drag C_{fd} coefficients.

The extent of the changes in the total drag coefficient C_d with increasing the leading edge thickness is displayed in Fig. 6. It is apparent from this figure that as the leading edge becomes blunt the contribution of the pressure drag to the total drag increases and the contribution of the skin friction drag decreases. For the reference round leading edge case, the pressure drag C_{pd}, skin friction drag C_{fd} and total drag C_d coefficients are 1.352, 0.167 and 1.519, respectively. Thus, compared to the flat-nose leading edges, the reference round leading edge presents high value to the total drag coefficient, where the major contribution is given by the pressure drag coefficient. As a reference, the total drag for the reference round leading edge is 1.49, 1.45 and 1.37 times larger than those for thickness t/λ_∞ of 0.01, 0.1 and 1, respectively.

4.2 Round Leading Edge

In order to compare flat-nose leading edge with round leading edge, it becomes necessary to determine the dependence of the heat transfer and total drag for round leading edge on the nose radius. In this way, DSMC simulations were performed for four round leading edges, besides the reference round leading edge (circular cylinder), with nose radii R_N/λ_∞ of 0.02, 0.1, 1.0, and 2.0, which correspond to overall Knudsen number Kn_D of 25, 5, 0.5 and 0.25, respectively, by assuming the nose diameter as the characteristic length.

Distributions of the heat transfer coefficient C_h along the round leading edge surface are

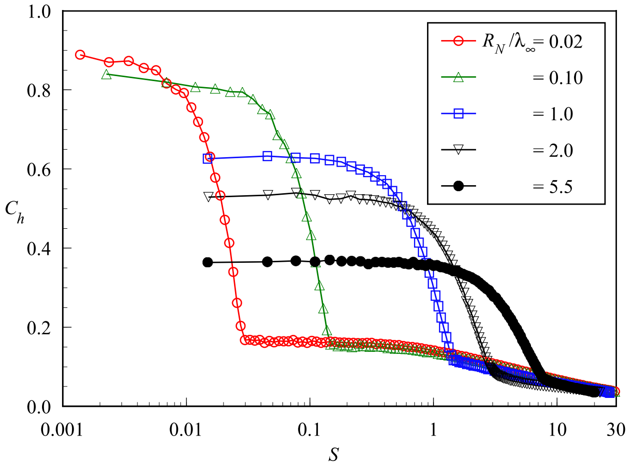

Fig. 7 Heat transfer coefficient along the round leading edge surface for various nose radii.

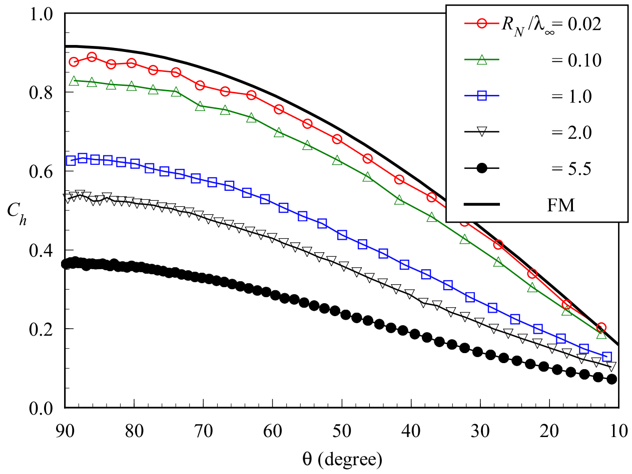

Fig. 8 Heat transfer coefficient along the cylindrically blunt portion of the round leading edge as a function of the body slope angle.

demonstrated in Fig. 7 with the dimensionless nose radius R_N/λ_∞ as a parameter. It is observed from this figure that altering the nose radius produces a substantial change in the heat transfer coefficient in the cylindrically blunt portion of the leading edge, provided that the gas-surface interaction is diffuse. The heat transfer coefficient presents the maximum value in the stagnation point and drops off sharply along the cylindrically blunt portion up to the cylinder/wedge junction. Also, the heat transfer coefficient in the stagnation region decreases with increasing the nose radius. This behavior seems to be in agreement with the continuum predictions for blunt body in that the heat flux scales inversely with the square root of the nose radius.

The nose radius effect can also be seen in a different way by comparing the DSMC computational results with those calculated by assuming free molecular flow. Figure 8 presents this comparison for the heat transfer coefficient as a function of the body slope angle θ. These curves indicate that the heat transfer coefficient approaches the free molecular limit ($C_{ho} = 0.915$) in the cylindrically portion of the round leading edge with reducing the nose radius.

The heat transfer coefficient at the stagnation point C_{ho}, obtained by a curve fitting process performed over the curves displayed in Fig. 8, corresponds to 0.883, 0.824, 0.630, 0.532 and 0.366 for round leading edges with nose radii R_N/λ_∞ of 0.02, 0.1, 1.0, 2.0, and 5.5, respectively.

Distributions of the pressure coefficient C_p along the body surface for different nose radii are displayed in Fig. 9. According to this figure, it is seen that the pressure coefficient follows the same trend as that presented by the heat transfer coefficient. The pressure coefficient presents the maximum value at the stagnation point and decreases fast in the cylindrically blunt portion of the leading edge. It is also verified that the pressure coefficient in the cylindrically blunt portion is one order of magnitude higher than the pressure coefficient in the wedge portion of the leading edge.

Variations of the skin friction coefficient C_f caused by changes in the nose radius of the leading edge are demonstrated in Fig. 10 as a function of the dimensionless arc length S. As can be seen, the skin friction coefficient increases from zero at the stagnation point to a maximum that is located in the cylindrically blunt portion of the leading edge, and decreases downstream along the body surface. Similarly to the flat-nose shapes, the round leading edges also exhibit the maximum value for the skin friction coefficient around a 45-degree station.

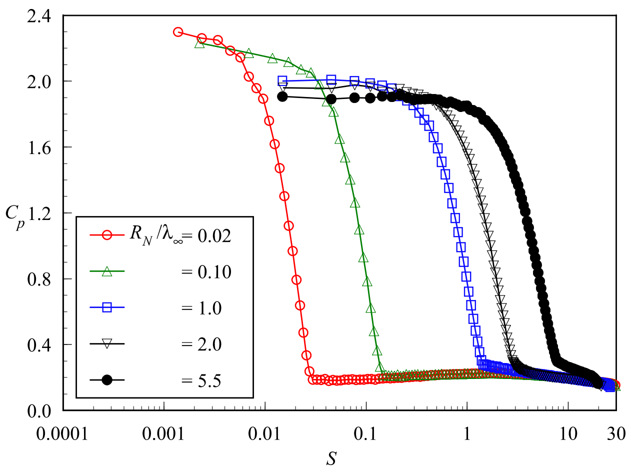

Fig. 9 Pressure coefficient along the round leading edge surface for various nose radii.

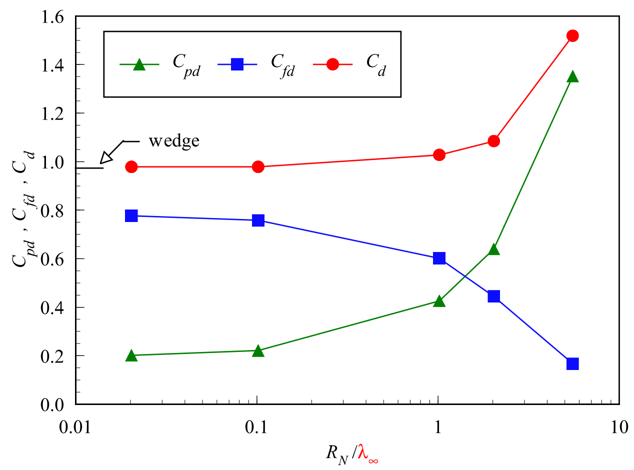

Fig. 11 Total drag coefficient for round leading edges as a function of the nose radius.

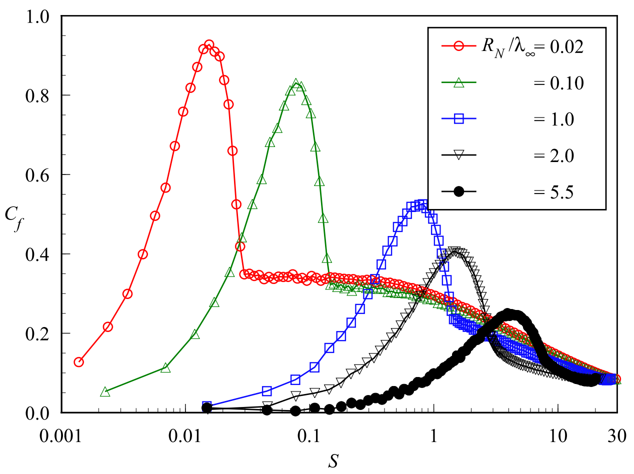

Fig. 10 Skin friction coefficient along the round leading edge surface for various nose radii.

The dependence of the total drag coefficient C_d on the nose radius is depicted in Fig. 11. In this figure, the contributions of the pressure drag C_{pd} and the skin friction drag C_{fd} coefficients are also shown. As would be expected, the total drag for round leading edges approaches the wedge drag with decreasing the nose radius.

4.3 Equivalent Nose Radius

The stagnation point heating and the total drag for flat-nose leading edges have been compared to those for the reference round leading edge in the previous sections. A second means of comparison between flat-nose shapes and round leading edges is defined as equivalent round leading edge. Equivalent round leading edges, or equivalent nose radii, are found that have the same value of stagnation point heating or total drag provided by the flat-nose leading edges. For instance, by holding the stagnation point heating the same, the total drag on the equivalent round leading edge may be compared to those for flat-nose leading edges in order to determine which shape is better suited for leading-edge blunting.

A summary of the computed data for the heat transfer coefficient C_{ho} at the stagnation point and the total drag coefficient C_d for the round leading edges is displayed in Fig. 12.

The stagnation point heating C_{ho} for each one of the flat-nose shapes is used as an input in Fig. 12 in order to determine the equivalent nose radius $R_{N,eqv}$. With the equivalent nose radius, the total drag that corresponds to this equivalent nose radius is also obtained from Fig. 12 itself.

The comparison of the total drag coefficient for flat-nose shapes $C_{d,fn}$ and for round leading edges with equivalent nose radii $C_{d,eqv}$ that match flat-nose body stagnation point heating is tabulated in Table 2. In this table, subscripts fn and eqv stand for flat-nose and equivalent round leading edges, respectively. For comparison pur-

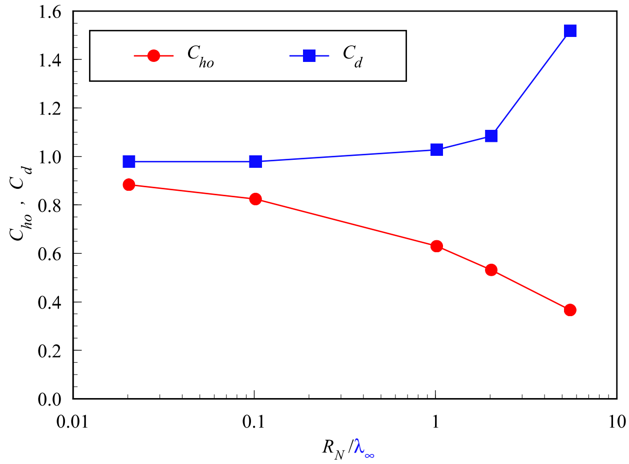

Fig. 12 Heat transfer coefficient C_{ho} at the stagnation point and the total drag C_d for round leading edges as a function of the nose radius.

Table 2 Nose radius necessary for comparable stagnation point heating to flat-nose shapes.

Kn_t	$\frac{t}{\lambda_\infty}$	$\frac{R_{N,eqv}}{\lambda_\infty}$	$\frac{R}{R_{N,eqv}}$	$\frac{C_{d,eqv}}{C_{d,fn}}$	$\frac{V_{eqv}}{V_{fn}}$
100	0.01	0.064	86.77	0.957	1.121
10	0.10	0.334	16.60	0.948	1.181
1	1.0	1.869	2.96	0.973	1.245

Table 3 Nose radius necessary for comparable total drag to flat-nose shapes.

Kn_t	$\frac{t}{\lambda_\infty}$	$\frac{R_{N,eqv}}{\lambda_\infty}$	$\frac{R}{R_{N,eqv}}$	$\frac{C_{ho,eqv}}{C_{ho,fn}}$	$\frac{V_{eqv}}{V_{fn}}$
100	0.01	0.916	6.05	0.764	1.097
10	0.10	1.334	4.15	0.773	1.131
1	1.0	2.198	2.52	0.957	1.198

pose, the volume V associated with the shapes is also shown in Table 2. Volume is another important geometric comparison, which is related to the active cooling system that may be placed within the leading edge for the purpose of heat absorption. Referring to Table 2, it is noted that equivalent round leading edges have lower drag (around 5% of difference) than flat-nose bodies. In addition, equivalent round leading edges provide larger volume than flat-nose shapes. As a reference, the Kn_t = 1 case, which is tangent to a 10-degree wedge (see Fig. 1, has the same stagnation point heating as a round leading edge that is 2.96 times smaller than the reference round leading edge that is also tangent to the wedge at the same point. Moreover, this equivalent round leading edge has a volume that is 24.5% larger than the corresponding flat-nose body, the Kn_t = 1 case. Consequently, based on Table 2, for the same stagnation point heating, round leading edges perform slightly better than flat-nose bodies.

By using the total drag coefficient C_d found previously for flat-nose leading edges, an equivalent nose radius $R_{N,eqv}$ may be found from Fig. 12 that gives the same total drag coefficient as the flat-nose bodies. At this time, the stagnation point heating will be the important factor in order to determine which shape is better suited for leading-edge blunting.

The comparison of the stagnation point heating for flat-nose shapes $C_{ho,fn}$ and for round leading edges with equivalent nose radii $C_{ho,eqv}$ that match flat-nose body total drag is tabulated in Table 3. It is clear from Table 3 that equivalent round leading edges have lower stagnation point heating than the flat-nose bodies. Again, by taking the Kn_t = 1 case as a reference, this shape has the same total drag as a round leading edge that is around 2.52 times smaller than the reference round leading edge. Also, this equivalent round leading edge has a volume that is 19.8% larger than the corresponding flat-nose body. As a result, based on Table 3, round leading edges perform better than flat-nose bodies as the total drag consideration is involved.

5 Conclusions

The computations of a rarefied hypersonic flow on blunt leading edges have been performed by using the Direct Simulation Monte Carlo method. The calculations provided information concerning the nature of the stagnation point heating and total drag for a family of contours composed by a flat nose followed by a highly curved afterbody surface. The emphasis of the investigation was to compare these flat-nose leading edges with round leading edges in order to determine which geometry is better suited as a blunting profiles.

The aerodynamic performance of these flat-nose shapes was compared to a reference round leading edge (circular cylinder), typically used in blunting sharp leading edges for heat transfer considerations. It was found that the stagnation point heating is higher and the total drag is lower on the flat-nose shapes than the representative circular cylinder solution in this geometric comparison. These flat-nose leading edges behave as if they had a sharper profile than their representative circular cylinder. However, these shapes have more volume than the circular cylinder geometry. Hence, although stagnation point heating on these new shapes may be higher, the overall heat transfer to these leading edges may be tolerate if there is active cooling because additional coolant may be placed in the leading edge.

Moreover, equivalent round leading edges were defined with the same stagnation point heating or total drag yielded by the flat-nose leading edges. With the same stagnation point heating as flat-nose shapes, round leading edges were shown to produce slightly smaller total drag. In addition, for the same total drag, round leading edges gave smaller stagnation point heating than flat-nose leading edges. Hence, if stagnation point heating and drag are considered the primary issues in leading-edge design of hypersonic configuration, then round leading edges are superior to flat-nose leading edges.

However, shock standoff distance on a cylinder scales with the radius of curvature, therefore cylindrical bluntness added for heating rate reduction will also tend to displace the shock wave. The displacement of the shock wave is especially undesirable in a waverider geometry [7], because these hypersonic configuration usually depends on shock wave attachment at the leading edge to achieve its high lift-to-drag ratio at high-lift coefficient. In addition, shock wave detachment will allow pressure leakage from the lower surface of the vehicle to the upper surface, thereby degrading the aerodynamic performance of the vehicle. In this context, as the new shapes behave as if they were sharper profiles than the round leading edge (cylindrical bluntness), they may display smaller shock detachment distances than the corresponding round shapes. Nevertheless, the shock wave structure on these new shapes is the subject for future work.

References

[1] Reller Jr., J. O., "Heat transfer to blunt nose shapes with laminar boundary layers at high supersonic speeds", NACA RM-A57FO3a, 1957.

[2] Schaaf, S. A. and Chambre, P. L., *Flow of rarefied gases*, Princeton Aeronautical Paperbacks, Princeton University Press, Princeton, NJ, 1961.

[3] Bird, G. A.,*Molecular gas dynamics and the direct simulation of gas flows*, Oxford University Press, Oxford, England, UK, 1994.

[4] Bird, G. A., "Monte Carlo simulation in an engineering context", in *Progress in Astronautics and Aeronautics: Rarefied gas Dynamics*, edited by Sam S. Fisher, Vol. 74, part I, AIAA New York, 1981, pp.239-255.

[5] Borgnakke, C. and Larsen, P. S., "Statistical collision model for Monte Carlo simulation of polyatomic gas mixture", *Journal of computational Physics*, vol. 18, No. 4, 1975, pp.405-420.

[6] Santos, W. F. N., "Aerodynamic heating on blunt nose shapes in rarefied hypersonic flow", in *17th International Congress of Mechanical Engineering COBEM 2003*, 10-14 November 2003, São Paulo, SP, Brazil.

[7] Nonweiler, T. R. F.,"Aerodynamic problems of manned space vehicles," *J. of the Royal Aeronautical Society*, Vol. 63, Sept, 1959, pp.521-528.